Characterization of the Surface Enhanced Raman Scattering (SERS) of Bacteria

W. R. Premasiri*

The Photonics Center, Boston University, Boston, Massachusetts 02215

D. T. Moir

Microbiotix Incorporated, Worcester, Massachusetts 01605

M. S. Klempner

Boston University Medical Center, Boston, Massachusetts 02118

N. Krieger

West Rock Associates, Jamaica Plain, Massachusetts 02130

G. Jones II and L. D. Ziegler*

Department of Chemistry and The Photonics Center, Boston University, Boston, Massachusetts 02215

Received: June 22, 2004; In Final Form: September 28, 2004

The surface enhanced Raman scattering (SERS) of a number of species and strains of bacteria obtained on novel gold nanoparticle (∼80 nm) covered SiO_2 substrates excited at 785 nm is reported. Raman cross-section enhancements of $>10^4$ per bacterium are found for both Gram-positive and Gram-negative bacteria on these SERS active substrates. The SERS spectra of bacteria are spectrally less congested and exhibit greater species differentiation than their corresponding non-SERS (bulk) Raman spectra at this excitation wavelength. Fluorescence observed in the bulk Raman emission of *Bacillus* species is not apparent in the corresponding SERS spectra. Despite the field enhancement effects arising from the nanostructured metal surface, this fluorescence component appears "quenched" due to an energy transfer process which does not diminish the Raman emission. The surface enhancement effect allows the observation of Raman spectra of single bacterial cells excited at low incident powers and short data acquisition times. SERS spectra of *B. anthracis* Sterne illustrate this single cell level capability. Comparison with previous SERS studies reveals how the SERS vibrational signatures are strongly dependent on the morphology and nature of the SERS active substrates. The potential of SERS for detection and identification of bacterial pathogens with species and strain specificity on these gold particle covered glassy substrates is demonstrated by these results.

Introduction

The well-known Raman cross-section enhancement effect arising from the proximity of nanostructured metal surfaces, i.e., surface enhanced Raman scattering (SERS), has been exploited in many studies to observe trace amounts of biologically relevant molecules.[1−9] The ability to provide a unique vibrational signature of a biologically or medically relevant species lacking any visible chromophores in aqueous solution at low concentrations illustrates the potential that SERS has to be a valuable analytical and structural spectroscopic tool. In particular, the development of SERS for the detection and identification of bacterial pathogens has attracted recent research interest[10−16] motivated by both applications in clinical diagnostic microbiology and the current heightened concerns about potential bioterrorist attacks. Methods are urgently needed to identify pathogens rapidly and reliably in such settings. SERS spectra of some Gram-positive and Gram-negative bacteria on a novel gold nanoparticle covered SiO_2 substrate grown from metal ion doped sol−gels are shown here and illustrate how the attributes of SERS are well suited for these purposes.

Non-SERS or bulk Raman spectra of bacteria have previously been reported during the past decade.[17−25] Many of these studies have demonstrated that whole-cell Raman vibrational fingerprints can serve as the basis for classification and identification of intact bacterial cells when reliable and reproducible protocols can be established. Combined with data mining techniques for pattern recognition employing reference libraries, these vibrational fingerprints can be used to identify bacterial pathogens with species and, in some cases, strain specificity.[22−26] The speed, specificity, and relative ease of experimental implementation make this vibrational spectroscopic approach a potentially attractive alternative to current methodologies, such as polymerase chain reaction (PCR) based techniques,[27] for microorganism identification.

However, SERS should offer several advantages over bulk Raman observations for bacterial detection and identification purposes. For example, as a result of enhanced Raman cross-sections vibrational signatures may be obtained with greatly reduced data accumulation times and incident laser powers

* To whom correspondence should be addressed. E-mail: ranjith@bu.edu, lziegler@chem.bu.edu.

10.1021/jp040442n CCC: $30.25
Published on Web 12/16/2004

leading to the rapid observation of Raman spectra at the single cell level and the development of low cost portable Raman instrumentation. Owing to the metal surface proximity dependence of the SERS enhancement mechanisms, only cellular surface constituents within approximately 10 nm can be expected to contribute to SERS spectra.[28] The resulting anticipated molecular selectivity in the SERS spectra of bacteria, as compared to the corresponding bulk Raman vibrational signatures, may be a useful feature for the development of both analytical and structural probes of these microorganisms. This proximity effect, for example, has been previously exploited in SERS studies of photosynthetic plant membranes.[29] Other important benefits of the SERS methodology include reduced masking fluorescence[27,30,31] or water scattering contributions to the vibrational Raman spectra. The extent to which these features are evident in bacterial SERS spectra due to the gold nanoparticle covered SiO_2 chips employed here is illustrated below.

The more widespread implementation of SERS-based methodologies for microorganism identification, in general, has been questioned on the basis of the reproducibility and reliability of these vibrational signatures owing to the very sensitive dependence of this enhancement phenomenon on the microscopic morphology and stability of the SERS active substrate.[14,16,32,33] SERS spectra have been previously reported for bacteria in silver and gold colloid solutions,[10,14] bacteria placed on electrochemically roughened metal surfaces,[13,15] bacteria coated by silver metal deposits,[11,12] and bacteria co-deposited with silver colloid aggregates on inert substrates.[16] The corresponding bacterial SERS spectra appearing in these reports vary considerably both in terms of absolute enhancement and relative band intensities when comparisons are possible for a given species. Recently, various sol−gel-based recipes incorporating metal colloids have been shown to result in successful SERS substrates.[32,34−40] Large Raman enhancements have been found for nanosized metal particles dispersed in the resulting gel structure, in part, due to the large stabilized metal surface areas available to molecular-sized scatterers. In contrast, the sol−gel-derived SiO_2 SERS substrate produced by the procedure described here is covered by immobilized clustered aggregates of monodisperse-sized gold nanoparticles grown in situ. Large, reproducible Raman vibrational enhancements are found (vide infra) for bacteria placed on these novel SERS substrates.

SERS spectra have been obtained from Gram-positive bacteria *Bacillus cereus*, *Bacillus subtilis*, *Bacillus anthracis* Sterne (a nonvirulent strain), and *Bacillus thuringiensis* and Gram-negative bacteria *Escherichia coli* and *Salmonella typhimurium*, placed on the in situ grown, aggregated gold particle covered SiO_2 chips developed here. The characteristics of these bacterial SERS spectra described in this report are as follows: (1) the magnitude of the bacterial Raman enhancement effect and the reproducibility currently obtainable on these gold particle covered SiO_2 chips; (2) the contrast between the SERS and bulk (non-SERS) Raman spectra of these microorganisms; (3) the ability to obtain single cell level Raman spectra on these SERS active substrates; (4) the SERS bacterial fluorescence "quenching" effect seen for some of these species; (5) the species, strain, and mutation specificity obtained in the SERS vibrational signatures; and (6) a comparison of our SERS results with previously reported bacterial SERS observations.

Experimental Section

SERS Active Substrate. The SERS active substrate used to obtain the spectra reported here is an aggregated gold nanoparticle coated SiO_2 matrix produced by a multistep in situ growth procedure. A gold ion doped sol−gel was formed by the hydrolysis of tetramethoxysilane in an acidic methanol solution (10 mL of HPLC grade methanol/5 mL of H_2O/3 mL of $Si(OCH_3)_4$ 99.99% Sigma) of $HAuCl_4$ (50 μL of ∼1 M $HAuCl_4$ 99.99% Sigma) as in previous procedures for the formation of metal-doped sol−gels.[35,37] Aliquots (25 μL) in polypropylene microcentrifuge tubes were dried in a fume hood for 12−48 h at ambient temperature and airflow. After exposure to water-saturated air for ∼1 h, the gel pellets are vigorously mixed (∼30 s) with 0.66 mM aqueous sodium borohydride (99.99% Sigma). This first rapid reduction step provides Au seeds for subsequent nanostructured metal particle growth. The solution is drained, and 50 mL of H_2O is added to the resulting gel pellets or chips. After 30 min of gentle shaking, the substrates are left in the greatly diluted $NaBH_4$ solution for ∼24 h. This second reduction stage promotes the slow growth of aggregated Au nanoparticles on the exposed SiO_2 surface almost exclusively during this period.

In contrast to previous sol−gel-based SERS substrates,[34−40] this procedure results in aggregates of monodisperse, nanosized gold spheres coating the outer surface of the resulting gel (monolith) matrix. Scanning electron microscopy (SEM) images (JEOL 6100 scanning electron microscope) of the SERS substrates resulting from this doped sol−gel procedure are shown in Figure 1. An SEM image of a two-cell chain of a bacterium (*B. anthracis* Sterne) on this Au particle covered SERS substrate is displayed in Figure 1a. The surface roughness scale in comparison to typical bacterial dimensions (∼μ) is evident in this image. Note that bacterial dimensions are conveniently on the order of the (near diffraction limited) spatial resolution obtainable with conventional commercial Raman microscope instrumentation. When the SEM image of the SERS substrate is viewed at an order of magnitude higher magnification, clusters of 1−15, ∼80 nm Au particles can be seen covering the solid SiO_2 surface as shown in Figure 1b. When the SERS substrate is cleaved and oriented such that both the surface and the interior of the glass chip can be viewed in the SEM image (Figure 1c), the Au nanoparticles, which appear as bright features in the SEM, are only evident on the outer surface of the SiO_2 substrate. Only the dark SiO_2 region is evident below the metal-covered outer surface at this SEM resolution (greater than ∼50 nm).

Raman Instrumentation. A Renishaw Raman microscope (model RM-2000) capable of ∼2λ spatial resolution was used to observe the scattering excited by a 785 nm diode laser. Typically, the incident laser power was attenuated to 1−3 mW and the spectral data acquisition time was in the 1−10 s range to obtain the SERS spectra of bacteria reported here. Spectral resolution was usually set to 3 cm^{-1} for this cooled CCD (400 × 578 array size) detection system (0.25 M spectrometer fitted with a 1200 groove/mm grating). The frequency calibration was set by reference to the 520 cm^{-1} vibrational band of a silicon wafer. Most of the Raman data (SERS and bulk) were obtained with a 50× microscope objective for Raman excitation/collection. Single cell level spectra, however, were acquired with a 100× objective.

Bacterial Sample Preparation and Handling. The following bacterial strains were obtained from the sources indicated and used in this study: *E. coli* K12 (12-4500), *S. typhimurium* (15-5351A), *B. cereus* (15-4869), and *B. thuringiensis* (15-4926) were obtained from Carolina Biological Supply (catalog numbers noted). *B. anthracis* Sterne was obtained from the Colorado Serum Co.; *B. subtilis* YS11 was from the Bacillus Genetic Stock Center (BGSC); *B. subtilis* 3610 (SSB2) and its congenic

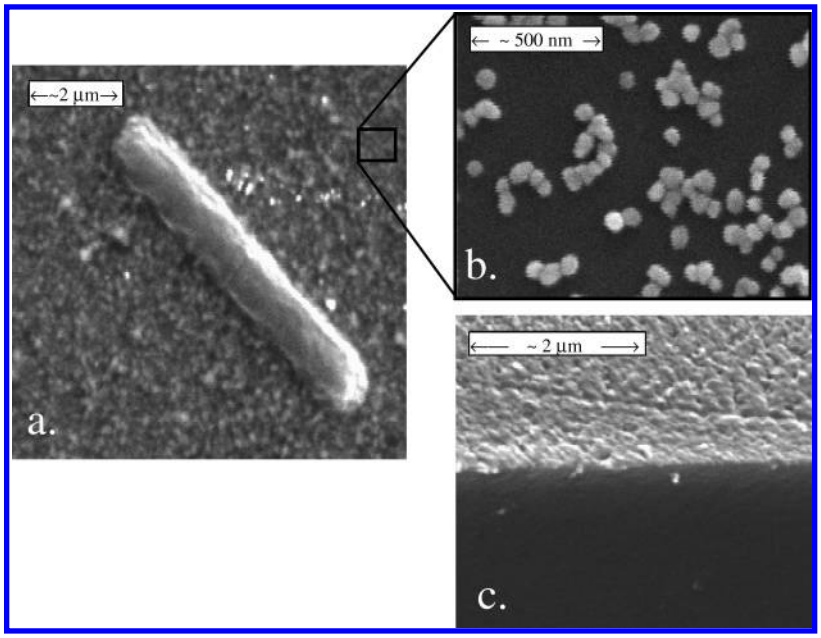

Figure 1. (a) A scanning electron micrograph of a two-cell chain of *B. anthracis* Sterne bacteria on a gold nanoparticle covered SiO_2 SERS chip. Note the relative size scales of the bacterium and the nanostructured surface roughness. (b) An SEM image of this SERS substrate at ~10-fold enhanced magnification. Clusters of 1−15 ~80 nm Au particles are evident on the surface of the SiO_2 SERS substrate. (c) An SEM image of this cleaved SERS substrate looking toward the cleaved edge of the substrate. Nanostructured metal regions are bright in the SEM; SiO_2 appears only as a dark region. Nanosized Au particles are only evident on the surface of this SiO_2 chip as evidenced by the bright region in the top half of the image. The SiO_2 exposed by the substrate cleavage is dark below this region.

insertion deletion construct *hag::erm* (SSB71) were provided by Drs. S. Branda and R. Kolter (Department of Microbiology and Molecular Genetics, Harvard Medical School). The *B. anthracis* Sterne *cotE::cat* mutant was provided by Adam Driks (Department of Microbiology and Immunology, Loyola University Medical Center). Bacterial cells were grown in 5 mL of LB (Sigma) broth (~5 h) to an $OD_{600} = \sim 1$, washed five times with water, and resuspended in 0.25 mL of water. About 1 μL of the bacteria suspension is placed on the SERS active substrate using a loop. The time lapse between placing the samples on the SERS surface and taking the Raman measurement is about 2 min. Bulk or non-SERS bacterial samples, excited with about 300 mW at 785 nm, were correspondingly placed on KBr.

Standard biosafety level 2 lab procedures were employed for handling the strains studied here even though they are nonvirulent. Residual spore-forming bacteria were destroyed by exposure to 2% hypochlorite solution for ~30 min. Non-spore-forming bacteria and contaminated glassware were autoclaved prior to disposal.

Results and Discussion

Bacterial Raman Cross-Section Enhancement Factor. Raman cross-section enhancements due to the proximity of nanostructured metal surfaces are typically cited in the range of 10^3-10^6 per molecule from ensemble averaged SERS measurements depending on the nature of the SERS active substrate, excitation wavelength, and Raman chromophore electronic structure.[28] Single molecule enhancements at selected "hot spots", however, as large as 10^{14} have been reported.[41−43] To provide some quantitative measure of the magnitude of the bacterial SERS enhancement on the gold particle covered substrates used here, the *relative* SERS and bulk (non-SERS) Raman scattering cross-sections, i.e., scattered power per bacterium, normalized for data collection time and incident laser power, of Gram-negative, *E. coli*, and Gram-positive, *B. anthracis* Sterne, bacteria were determined. The observed corresponding normalized SERS and bulk Raman spectra are compared in Figures 2 and 3. If we compare the strongest vibrational band in each spectrum, the Raman cross-section of *E. coli* is found to be amplified by a factor of 2×10^4 per bacterium on our Au particle covered SERS substrate (Figure 2). The non-SERS Raman spectrum of *B. anthracis* Sterne excited at 785 nm (Figure 3b) sits on top of a broad fluorescence feature as seen in Figure 3b. This fluorescence component is discussed further below. However, when the contribution due to this broad structureless emission feature is subtracted from the observed resonance emission, a Raman spectrum is evident (see Figure 3b). The *B. anthracis* Sterne Raman enhancement per bacterium due to our SERS substrate is found to be 5×10^4 for this Gram-positive species. This amplification factor is slightly larger than that for *E. coli*. These different per bacterium enhancement factors may be attributable to the different Gram-

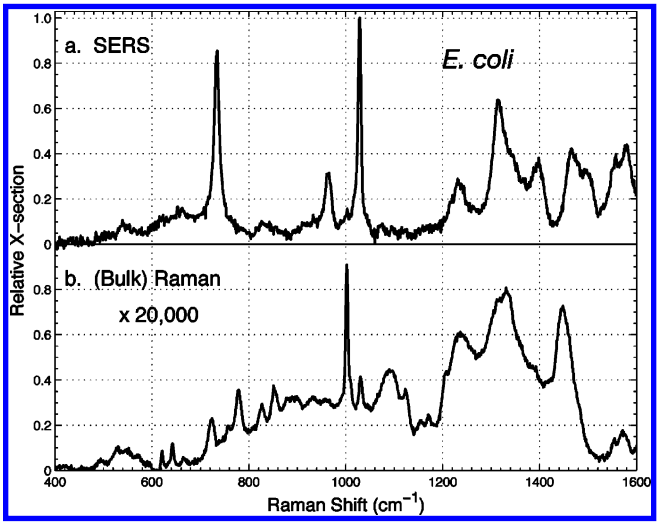

Figure 2. Comparison of the relative per bacteria Raman scattering cross-sections of the (a) SERS and (b) normal (bulk) Raman spectra of *E. coli* excited at 785 nm. The intensity of the normal Raman spectrum (b) has been multiplied by a factor of 20 000 to allow scattering cross-section comparisons on the same relative intensity scale.

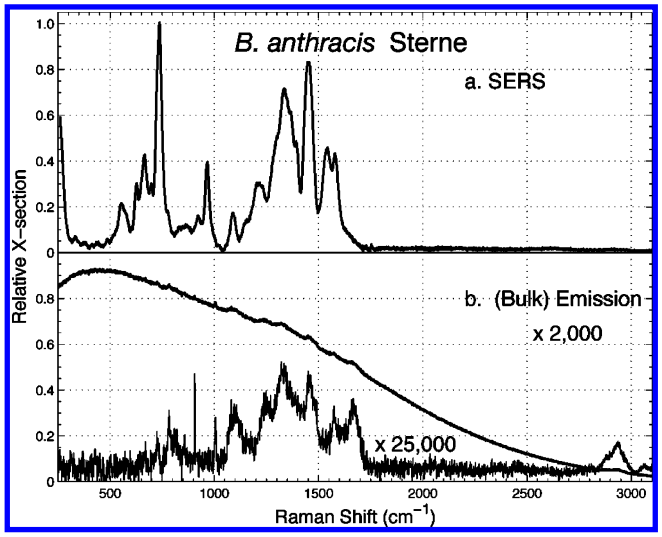

Figure 3. Comparison of the relative per bacteria Raman scattering cross-sections of the (a) SERS and (b) normal (bulk) non-SERS emission of *B. anthracis* Sterne excited at 785 nm. The intensity of the non-SERS (bulk) emission which exhibits both a Raman and a broad fluorescence component (b) has been multiplied by a factor of 2000. Also shown in panel b is the Raman spectrum that results when the broad fluorescence feature has been subtracted. This Raman spectrum has been multiplied by a factor of 25 000 to allow the scattering cross-section comparison with the corresponding SERS spectrum on the same intensity scale.

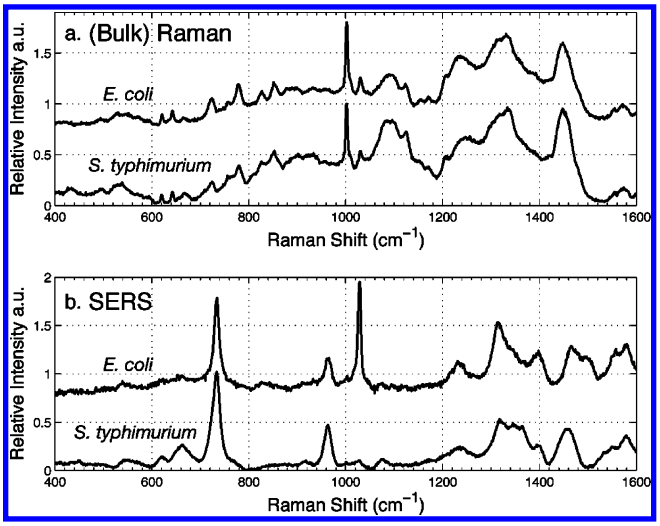

Figure 4. A comparison of the (a) non-SERS, bulk Raman spectra and the (b) SERS spectra of *E. coli* and *S. typhimurium*. *E. coli* spectra are displaced vertically for viewing. All spectra have been normalized by the height of the most intense band in each spectrum. More spectral distinction is evident in the SERS spectra than in the corresponding non-SERS spectra.

positive and Gram-negative cell surface structures of these two bacterial species. Alternatively, the near resonant electronic character, as evident by the fluorescence emission, may contribute to a larger "chemical enhancement" effect for the SERS cross-section of *B. anthracis* Sterne derived at this excitation wavelength. The bulk Raman spectra of both species (Figures 2b and 3b) were obtained with 300 mW of incident 785 nm excitation power and 100 s signal accumulation times. The corresponding SERS spectra (Figures 2a and 3a) were excited with 2 mW and collected in 10 s. The displayed spectra are single scans. The relative number densities of bacteria contributing to the bulk (∼500) and SERS (∼25) spectra in Figures 2 and 3 were estimated from the known scattering volume ($3\mu \times 30\mu \times 20\mu$) and the bacterial dimensions. Only a bacterial monolayer was assumed to contribute to the SERS spectra.

Determination of the magnitude of the Raman enhancement factor per bacterial cell provides a means for quantitative evaluation of the Raman amplification efficiency as a function of experimental parameters such as SERS substrates, bacterial species, excitation wavelength, and so forth and hence allows critical comparisons with substrates prepared in different laboratories. Finally, it should be emphasized that this per bacterium enhancement factor (here in the range of $2-5 \times 10^4$) is not a measure of the per molecule SERS enhancement more typically quoted in the SERS literature because only those correctly oriented molecules close to the SERS active substrate, presumable some fraction of cell surface components, are enhanced. Vibrational bands due to these outer surface components may contribute only weakly to the observed bulk Raman spectrum excited at 785 nm which is determined by both cytoplasmic as well as all surface layer components. The SERS enhancement factors reported here are thus, necessarily, lower estimates of the per molecule Raman enhancement effect arising from these gold-covered SiO_2 substrates.

Comparison of SERS and Non-SERS Spectral Features. Due to the distance and orientation dependence of the electromagnetic and charge-transfer enhancement mechanisms, only those molecular components close to the SERS active surface (within ∼10 nm) with the correct orientation are preferentially enhanced.[28,29] Thus, the number of vibrational bands and the relative intensities of these vibrational features can be expected, in general, to be different in the SERS and non-SERS Raman vibrational signatures of bacteria. Our observations substantiate these expectations. For example, the non-SERS or bulk Raman vibrational spectra of *E. coli* and *S. typhimurium*, normalized to the intensity of the most intense band in each spectrum, are shown in Figure 4a, and the corresponding first derivatives of these spectra are given in Figure 5a,b. The bulk spectra of these two bacterial species are extremely similar, judging by the peak positions and relative intensities. Previously reported non-SERS Raman spectra of other bacterial species also show a striking spectral resemblance to one another.[22,23,25] However, greater species differentiation is evident in the normalized SERS spectra of these two species (Figure 4b) and the corresponding first derivatives of these spectra (Figure 5d,e). A more distinct species-specific vibrational spectral signature is seen in the SERS spectra than the corresponding bulk Raman spectra. For example, the relative intensities of a band at 1050 cm^{-1} and the relative intensity pattern in the 1200−1700 cm^{-1} region are obvious spectral differences between the SERS spectra of these two closely related species, in contrast to the bulk Raman spectra (Figure 4). When the *E. coli* and *S. typhimurium* SERS and bulk first derivative difference spectra are compared (panels c and f of Figure 5), more robust and obvious features are found for the SERS derivative difference spectrum than for the derivative difference spectrum of the bulk Raman signals. The greater Raman differentiation between species, which is more evident in the SERS spectra than in the corresponding bulk Raman spectra, apparently indicates that bacterial cells are more chemically distinct in their cell surface composition than in their cell cytoplasm, i.e., bacterial identity is more dependent on outer layer components than on the cellular machinery in the cytoplasm.

Furthermore, the number of Raman transitions in the SERS spectra of *E. coli* and *S. typhimurium* (Figure 4b) are significantly fewer than in the corresponding bulk Raman spectra for both of these bacterial species (Figure 4a). A more quantitative

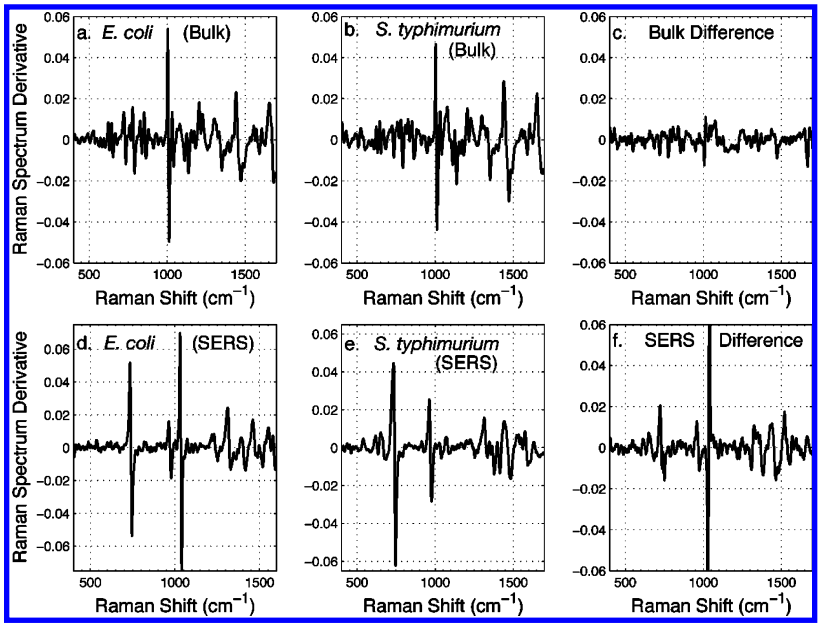

Figure 5. First derivatives of the bulk (non-SERS) and SERS spectra of *E. coli* and S. *typhimurium* given in Figure 4. The difference between the bulk and SERS spectra of these two species is displayed in panels c and f, respectively.

measure of this difference is evident when the number of zero crossings in the bulk and SERS first derivative Raman spectra of *E. coli* (Figure 5a,d) and *S. typhimurium* (Figure 5b,e) are compared. There are nearly twice as many vibrational bands, as judged by the zero crossings, for the bulk spectra as compared to the SERS spectra for these two species. This reduction in spectral congestion, coupled with the greater Raman differentiation in the SERS observation, makes the SERS technique potentially a more powerful spectroscopic tool than normal Raman for bacterial identification, aside from the advantages due to the enormously enhanced Raman scattering efficiency arising from the nanostructured metal surface effects.

Finally, comparison of the *E. coli* and *S. typhimurium* SERS and bulk Raman spectra (Figure 4 and Figure 5) reveals that the relative Raman intensities and frequencies of the SERS and non-SERS spectra *for a given species* can be quite different. For example, the strongest band in the SERS spectrum at 735 cm^{-1} is barely evident in the non-SERS spectrum and the intensity pattern in the 1200−1600 cm^{-1} region shifts considerably in the SERS spectra as compared to the corresponding bulk Raman spectra.

"Fluorescence Quenching". A comparison of the SERS spectrum and the bulk total spontaneous emission spectrum of *B. anthracis* Sterne excited at 785 nm illustrates an additional attribute of the SERS methodology. As shown in Figure 3b, the non-SERS emission spectrum of *B. anthracis* exhibits a relatively weak Raman spectrum spectrally overlapped by a more intense, broad fluorescence emission. A fluorescence quenching effect has often been attributed to SERS chromophores which are also electronically resonant by virtue of the incident Raman excitation frequency.[16] The local field enhancement resulting from the EM mechanism, which accounts for the bulk of the Raman cross-section amplification, also enhances the excitation and emission fields responsible for fluorescence from chromophores close to the metal nanostructure surface.[44−46] However, when a resonantly excited electronic state is brought close to a metal surface (nanostructured or flat), classical resonant dipole−dipole coupling results in rapid energy transfer from the excited state of the chromophore to the metal resulting in a shortened excited-state lifetime[47,48] (T_1) and a corresponding decreased fluorescence quantum yield. The competing distance dependent energy transfer and field enhancement effects result at most in a putative (less than a factor of 10) surface enhanced fluorescence (SEF) at some intermediate surface metal distance. The redistribution of resonant secondary radiation into Raman and fluorescence emission components is determined by the relative population decay of the resonant excited state and the pure-dephasing rate ($1/T_2$*) of the resonantly excited electronic transition.[49−51] (Pure-dephasing rates describe the time scale of the quasi-elastic solute−solvent bath interactions, i.e., a solvation dependent time scale). In the fast modulation limit, the ratio (integrated yield) of the fluorescence to Raman resonant emission is given by the ratio of the excited-state lifetime to the pure-dephasing time (i.e., $2T_1/T_2$*). Thus, although the field enhancement mechanism amplifies equivalently the Raman and fluorescence components from a resonantly excited chromophore, the SERS emission is dominated by the Raman component due to the decreased lifetime resulting from the energy transfer process. Although the pure-dephasing rate may be affected by the surface proximity, it must not be strongly increased as evidenced by the relative Raman and fluorescence yield of resonantly excited chromophores. In fact, it might be anticipated that the pure-dephasing rate decreases compared to the solution pure-dephasing rate upon adsorption to the SERS surface due to the more rigid environment of a physi-adsorbed species in contrast to free solution.

The above discussion only applies to the Raman and fluorescence emission components from an electronically resonant SERS chromophore. For a sample which consists of resonant and nonresonant chromophores, such as the 785 nm excited *B. anthracis* Sterne emission shown in Figure 3, the molecules accounting for the (electronically) nonresonant SERS signal only experience the usual surface field enhancement effects and the energy transfer (T_1) considerations are irrelevant.

Although the nature of the fluorescent species, i.e., impurity or inherent component, has not been established, a broad fluorescence is observed to overlap the Raman spectra for all of the *Bacillus* species examined in this study (*B. cereus*, *B. anthracis*, *B. subtilis*, and *B. thuringiensis*) when excited at 785 nm. This is in contrast to the bulk Raman scattering we have observed from non-*Bacillus* species grown in the same medium and excited at 785 nm (see Figures 2 and 4). However, whatever

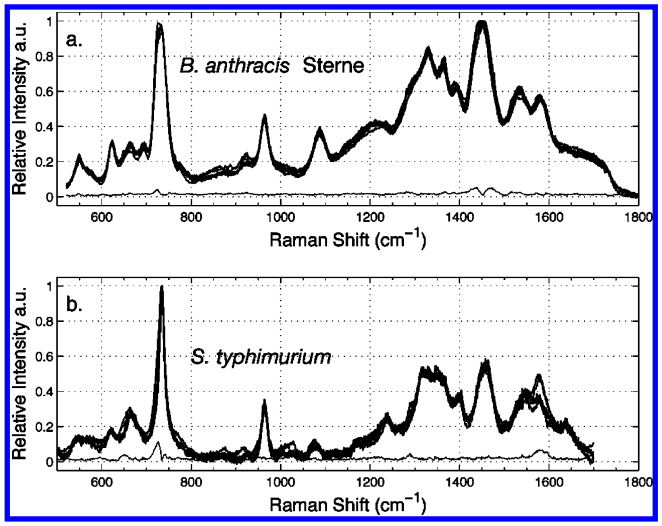

Figure 6. Six spectra of (a) *B. anthracis* Sterne and (b) *S. typhimurium* normalized by the peak intensity of the strongest vibrational feature (1450 cm^{-1}) are overlapped in order to demonstrate the SERS signal reproducibility on this Au particle covered substrate. Three spectra were obtained from different areas of the same SERS chip; three spectra were obtained from a different chip. The standard deviation spectrum for each of these species is shown at the bottom in each panel.

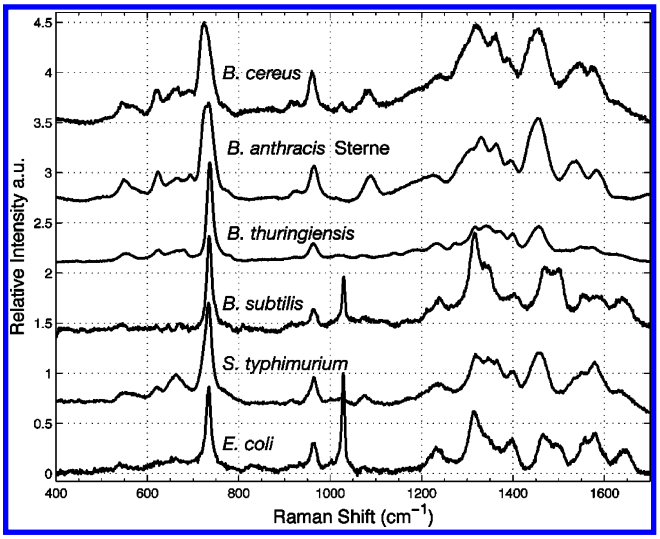

Figure 7. SERS spectra of six bacterial species obtained on gold aggregate coated SiO_2 chips. An incident laser power of 2 mW and a data accumulation time of 10 s were used to obtain these spectra. Spectra are offset vertically for display purposes and top-to-bottom ordered according to their phylogenetic relationship.

the nature of this fluorescent chromophore, the independence of SERS to energy transfer processes, as compared to fluorescence emission, results in the elimination of broad overlapping emission features which can otherwise mask the vibrational Raman signature (Figure 3). In particular, SERS is essential for the observation of high quality Raman vibrational signatures excited by red to visible radiation uncluttered by this overlapping broad emission component in potential priority pathogens such as *B. anthracis*.

SERS Reproducibility. One measure of the SERS spectral reproducibility obtainable with the clustered gold nanoparticle covered SiO_2 substrates is illustrated in Figure 6. As mentioned above, producing sensitive and reproducible substrates has been a major obstacle to the more widespread use of SERS for analytical applications. SERS spectra of *B. anthracis* Sterne and *S. typhimurium* acquired from three different locations on the same SiO_2 chip and from three different chips, normalized by the intensity of the strongest band in each spectrum, are overlapped in Figure 6. Corresponding standard deviation spectra for these data sets are also displayed in this figure. The *absolute* scattering intensities of the six spectra for each of these species vary by less than 15% at ~735 cm^{-1} (signal maximum). These results are typical for the SERS signals obtained for bacterial samples from the same culture or from cultures grown on different days in the same broth type and illustrate the degree of reproducibility already achieved with these novel SERS-inducing substrates. The observed differences are largely ascribed to the inhomogeneity of the metal particle coated SiO_2 chip surfaces produced by our current growth procedure. In addition, some smaller spectral differences here may result from the natural life cycle of these bacteria.

SERS of Bacteria: Species Specificity. SERS spectra of six species of bacteria in the 400−1700 cm^{-1} range acquired on the Au particle covered chips are shown in Figure 7. These are the results of single scans, and no additional averaging or smoothing has been applied to the spectra. They have been corrected only for the spectral response of the system and some baseline effects attributed to incident 785 nm radiation scattered from the SERS substrate surface itself. Due to the nature of the SERS enhancement mechanisms, SERS features in the carbon−hydrogen stretching region (2900−3200 cm^{-1}) of these bacteria are not observed (see Figure 3a) and thus only the 400−1700 cm^{-1} fingerprint region is included in this figure. Most critical to the application of SERS to bacterial pathogen detection and identification, each bacterial species is characterized by a unique SERS vibrational fingerprint, as seen in Figure 7. These bacterial spectra were obtained with ~2 mW of incident laser power in 10 s of data accumulation time. We estimate that these spectra result from the SERS activity of approximately 25−100 bacterial cells, depending on the species. These data demonstrate that SERS spectra of bacteria with excellent signal/noise (S/N) can be readily obtained when cells are placed on these aggregated Au particle coated substrates and excited by low laser power illumination at 785 nm.

The SERS spectra in Figure 7 are ordered from top to bottom according to their phylogenetic relationship; i.e., the more closely related species are adjacent to each other in this figure.[52] Systematic trends in spectral features correlated with this lineage are not obvious given the complex character of these fingerprints. Furthermore, SERS spectra of both Gram-positive, *B. anthracis* Sterne, *B. cereus*, *B. thuringienesis*, and *B. subtilis*, and Gram-negative, *E. coli* and *S. typhimurium*, species are shown in this figure. Again, somewhat surprisingly, obvious spectral differences attributable to these two classes of bacterial outer surfaces are not immediately striking. Phenomenologically, however, spectral regions with considerable homology can be discerned between closely related species. For example, SERS spectra of *B. anthracis* Sterne, *B. cereus*, and *B. thuringienesis* all exhibit a very similar pattern of relative intensities in the 1250−1650 cm^{-1} region. These bacteria are all closely related members of the *B. cereus* group.[53] Qualitatively, in the 500−1250 cm^{-1} region, a finite number of spectral bands are found to be in common with all these SERS bacterial signatures but their relative intensities vary. For example, bands at ~735, 965, 1030, 1080, and 1240 cm^{-1} are evident in different relative proportions in these SERS spectra (Figure 7). When these spectra are displayed on a higher resolution frequency scale, reproducible small frequency shifts and bandwidth changes are evident for some of these recurring vibrational bands. The relatively finite number of vibrational features that characterize these SERS spectra may serve as robust markers for identification algorithms. Finally, to underscore the species specificity

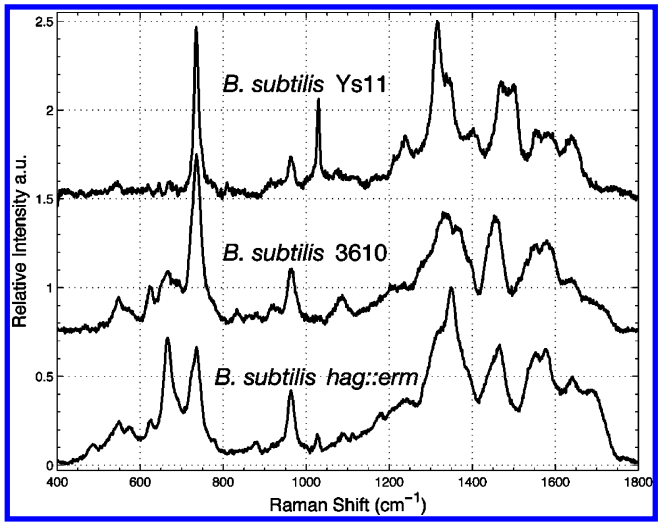

Figure 8. SERS spectra of wild-type *B. subtilis* 3610 cells, wild-type *B. subtilis* YS11 cells, and *B. subtilis* 3610 congenic mutant cells lacking flagella (*hag::erm*).

of these vibrational signatures, *B. anthracis*, *B. cereus*, and *B. thuringienesis* were found to be indistinguishable by their 16s rDNA sequences, generally considered to be the gold standard for bacterial identification.[53] However, the unique SERS signatures of the strains examined (Figure 7) unequivocally distinguish these closely related bacterial species.

A molecular level interpretation of these SERS vibrational features has not yet been established. Vibrational bands typical of proteins, phospholipids, nucleic acids, and polysaccharides are anticipated to contribute to these spectra. The ubiquitous strong bacterial SERS band at ~735 cm^{-1}, for example, has been attributed to the nucleic acid base adenosine in previous SERS studies of bacterial components.[13,40] However, the outer bacterial cell layer sensitivity of this spectroscopic technique makes the assignment of this band and features at 965, 1030, and 1080 cm^{-1} more likely arising from the lipid layer components of the cell walls and membranes.[16,54] Raman frequencies at 715 cm^{-1} (C−N stretching) and 1060 cm^{-1} (C−C stretching) are well-known markers of lipid layer fluidity, and vibrational bands in the 930−1130 cm^{-1} region have been also previously assigned to membrane phospholipids.[55] Amide I, II, and III vibrations, associated with protein backbone, and carboxylic stretches are expected in the 1220−1660 cm^{-1} region and probably dominate the SERS vibrational signature in this region.

Strain and Mutant Specificity. In addition to the species differentiation demonstrated above for these SERS fingerprints, evidence of the strain and mutant specificity provided by SERS on these gold cluster covered substrates is shown in Figure 8 in which SERS spectra of two strains of *B. subtilis*, YS11 and 3610, are displayed. Although the parentage of most of the bands can phenomenologically be traced from one spectrum to the next, the vibrational signature of each strain is unique, providing a fingerprint for identification purposes. SERS spectral differences between specific gene deletion bacterial mutants and their congenic parents may also be observed. The SERS spectra of wild-type (WT) *B. subtilis* 3610 cells and a congenic mutant lacking flagella (*hag::erm*) are also compared in Figure 8. The relative intensities of these two spectra have been normalized by the intensity of the largest peak in each. The *hag* gene is deleted in this mutant and is replaced with an erythromycin drug resistance marker, resulting in the loss of flagella. This significant surface structure change is revealed in white light microscopic images of stained cells.[56] However, the effect of this flagellum deletion is also clearly evident by the significant differences in the two SERS spectra.

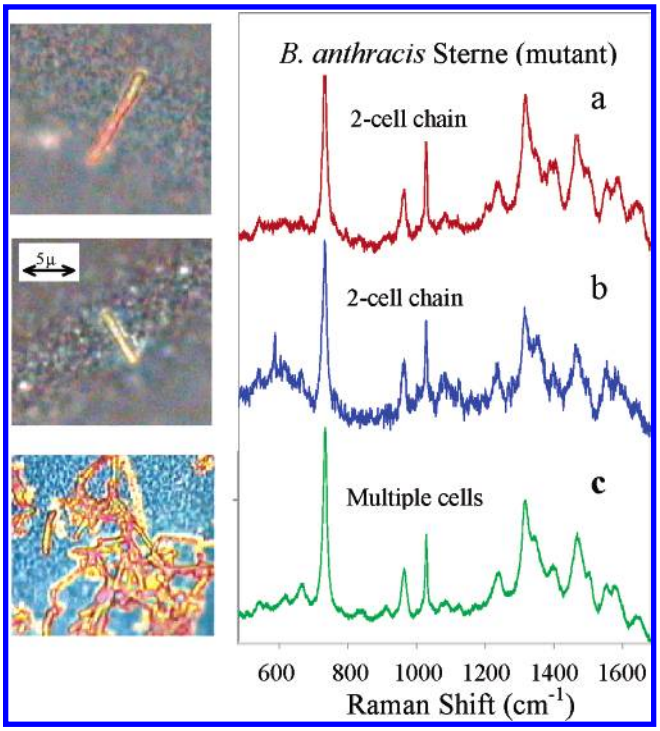

Figure 9. SERS spectra of a single *B. anthracis* Sterne (*cotE::cat* mutant) two-cell chain are shown in curves a and b. The corresponding SERS spectrum of multiple cells (~30) is given in curve c. The white light reflection image at the sampling volume is shown on the left for each of these scattering samples. The white light image verifies that only single organisms are contributing to the SERS spectra in curves a and b.

SERS at the Single Bacterial Cell Level. SERS spectra of bacteria at the single cell level are observed on our gold colloid cluster covered SiO_2 substrates. Aside from illustrating the sensitivity of this technique, the ability to observe vibrational signatures of single cells allows SERS to identify members of a mixture of cell types, thus enabling rapid detection and identification of mixed infection components and the study of heterogeneities of microbial populations in general. The SERS spectra of two different *B. anthracis* Sterne (*cotE::cat*) mutant)[57] two-cell chains are shown in Figure 9a,b. The corresponding white light images at the laser focal region, also shown in this figure, confirm that only a single bacterium was in the Raman illuminated volume during the SERS data collection period. The single cell level SERS spectra displayed in Figure 9 were observed when a 100× objective was used for excitation/collection, scattering data were accumulated for 20 s, and 3 mW of 785 nm incident laser power illuminated the sample. The *B. anthracis* SERS spectrum of a more concentrated multiple cell sample obtained with less tightly focused excitation (50× objective and a 10 s data accumulation time) is shown for comparison with the single cell level SERS spectra in Figure 9c. As the corresponding white light image shows (note the length scale change), the SERS spectrum in the lowest panel (c) is due to scattering of an ensemble averaged group of bacteria on the order of ~30 cells. The SERS spectra of the two-cell chains are quite similar to each other and to the "bulk" averaged SERS spectra.

The ability to observe single bacterial cell Raman signatures at low, nondamaging, incident powers (1−3 mW) and short illumination times (~10−30 s) derives from the scattering cross-section enhancement made possible by the metal surface field

amplification effects. SERS of a single human white blood cell on a vacuum-deposited gold island film was previously reported.[58] This cell (HL60) is about an order of magnitude larger than the bacterial cells of interest here, however, and nearly 3 times the incident 632.8 nm power and approximately 10 times longer data acquisition time were used to obtain this human blood cell SERS spectrum as compared to the single cell data reported here. Furthermore, FTIR spectroscopy of single cells is not a practical vibrational probe due to the diffraction limit of the longer IR wavelength and the inherently weak IR absorption cross-section. Non-SERS Raman spectra of a single bacterial cell (*Clostridium beijerinckii*) in a confocal microscopy configuration have appeared in a recent report.[20] However, longer illumination times and considerably higher ($\times$100) incident laser powers, which can damage less robust biological samples, are required to achieve S/N comparable to that achievable via the SERS methodology employed here.

Comparison with Previously Published SERS Spectra of Bacteria. As noted above, SERS spectra of some bacteria have been previously reported.[10−16] These spectra were obtained with two types of SERS substrates: bacteria coated, suspended, or co-deposited with Ag and Au colloids[10−12,14,16] and bacteria deposited on electrochemically roughened metal surfaces.[13,15] Qualitatively, the S/N of the bacterial SERS spectra obtained on our Au nanoparticle coated chips, normalized for the same collection times, appears significantly greater than in these previously published bacterial SERS spectra. When SERS spectra of the *same* species obtained from *different* SERS active substrates are compared with those reported here, large spectral differences are found. SERS spectra of these same bacterial species exhibit different patterns of relative intensities and frequencies on other SERS active substrates. For example, although many of the same vibrational bands appear in the SERS spectra of *E. coli* reported here and by Guzelian et al.[13] the two most intense features are at 714 and 1132 cm^{-1} in the Guzelian work and 732 and 1027 cm^{-1} in our spectra. In Jarvis and Goodacre,[16] a vibrational band at 652 cm^{-1} is the only intense feature below 1000 cm^{-1} (the only spectral region reported) in their SERS spectrum of *E. coli*. The reported SERS spectrum of silver-coated *E. coli*[11,12] is almost completely uncorrelated with the SERS spectrum obtained on our Au particle coated substrates. Thus the SERS signature of bacteria appears to be quite specific to the morphology of the SERS-promoting nanostructured metal surface.

Conclusions

The results presented here clearly demonstrate that high quality, i.e., excellent signal-to-noise and reproducible, Raman spectra of bacteria are obtained when the microorganisms are placed on the novel gold particle aggregate covered glass chips described here. Enhancement intensity factors are greater than 10^4 per bacterium, demonstrating that bacterial signatures are strongly amplified on these substrates. The bacterial SERS spectra are less spectrally congested and show greater differentiation as compared to bulk Raman spectra. The elimination of fluorescence emission, critical to detection and identification applications, is found to be important for *Bacillus* species excited in the NIR/red region. The bacterial SERS fingerprints clearly distinguish species and strains, and the ability to quickly obtain high quality Raman spectra of bacterial single cells should prove useful for interrogating the heterogeneity of bacterial populations in general and for distinguishing dangerous pathogens in a mixture more specifically.

The future molecular level challenges are clearly evident for this methodology as well. A combination of model compounds and genetically engineered mutants will be used to help identify the molecular origins of the observed vibrational signals. An additional subsequent goal is to exploit data mining techniques to develop algorithms to identify these pathogens in SERS spectra obtained from heterogeneous biological samples. Finally we note that additional separation techniques, such as centrifugation, will need to be incorporated into a bacterial detection and identification procedure based on SERS which allows the substantial isolation of bacterial-sized cells ($\sim$1 μm) from larger cells and molecular species which will be components of natural biological fluids. Efforts to demonstrate this capability are currently underway in our laboratory.

Acknowledgment. The support of the Army Research Laboratory (Cooperative Agreement DAAD19-00-2-0004, Task 17) and the Boston University Photonics Center is gratefully acknowledged. We thank S. Branda and R. Kolter (Department of Microbiology and Molecular Genetics, Harvard Medical School) for the gift of the *B. subtilis hag* insertion deletion construct and Adam Driks (Department of Microbiology and Immunology, Loyola University Medical Center) for the *B. anthracis* Sterne *cotE::cat* mutant.

References and Notes

(1) Cotton, T. M.; Kim, J. M.; Chumanov, G. D. *J. Raman Spectrosc.* **1991**, *22*, 729.
(2) Herne, T. M.; Ahern, A. M.; Garrrell, R. L. *J. Am. Chem. Soc.* **1989**, *113*, 846.
(3) Grabb, E. S.; Buck, R. P. *J. Am. Chem. Soc.* **1989**, *111*, 8362.
(4) Wantanabe, T.; Maeda, H. *J. Phys. Chem.* **1989**, *93*, 3258.
(5) Chumanov, G. D.; Efremov, R. G.; Nabiev, I. R. *J. Raman Spectrosc.* **1990**, *21*, 43.
(6) Vo-Dinh, T.; Houck, K.; Stokes, D. L. *Anal. Chem.* **1994**, *66*, 3379.
(7) Kneipp, K.; Kneipp, H.; Manoharan, H.; Hanlon, E. B.; Itzkan, I.; Desari R. R.; Feld, M. S. *Phys. Rev. E* **1998**, *57*, R6281.
(8) Weldon, M. K.; Morris, M. D. *Appl. Spectrosc.* **2000**, *54*, 20.
(9) Cavalu, S.; Cinta-Pinzaru, S.; Leopold, N.; Kieffer, W. *Biopolymers* (*Biospectrosc.*) **2001**, *62*, 341.
(10) Sockalinham, G. D.; Lamfarraj, H.; Beljebbar, A.; Pina, P.; Allouch, P.; Manfeit, M. *Proceedings of the European Conference on the Spectroscopy of Biological Molecules*; Kluwer Academic: Boston, 1999; p 599.
(11) Efrima, S.; Bronk, B. V.; Czege, J. *Proc. SPIE* **1999**, *3602*, 164.
(12) Zeiri, L.; Bronk, B. V.; Shabtai, Y.; Czege, J.; Efrima, S. *Colloids Surf., A* **2002**, *208*, 357.
(13) Guzelian, A. A.; Sylvia, J. M.; Janni, J. A.; Clauson, S. L.; Spencer, K. M. *Proc. SPIE* **2002**, *4577*, 182.
(14) Fell, N. F., Jr.; Smith, A. G. B.; Vellone M.; Fountain, A. W., III *Proc. SPIE* **2002**, *4577*, 174.
(15) Grow, A. E.; Wood, L. L.; Claycomb, J. L.; Thompson, P. A. *J. Microbiol. Methods* **2003**, *53*, 221.
(16) Jarvis, R. M.; Goodacre, R. *Anal. Chem.* **2004**, *76*, 40.
(17) Puppels, G. J.; de Mul, F. F. M.; Otto, C.; Greve, J.; Robert-Nicoud, M.; Arndt-Jovin, D. J.; Jovin, T. M. *Nature* **1990**, *347*, 301.
(18) Puppels, G. J.; Colier, W.; Olminkhof, J. H. F.; Otto, C.; de Mul, F. F. M.; Greve, J. *J. Raman Spectrosc.* **1991**, *22*, 217.
(19) Schuster, K. C.; Urlaubb, E.; Gapesa, J. R. *J. Microbiol. Methods* **2000**, *42*, 29.
(20) Schuster, K.; Reese, I.; Urlaub, E.; Gapes, J. R.; Lendl, B. *Anal. Chem.* **2000**, *72*, 5529.
(21) Maquelin, K.; Choo-Smith, L.-P.; van Vreeswijk, T.; Endtz, H.; Smith, B.; Bennett, R.; Bruining, H. A.; Puppels, G. J. *Anal. Chem.* **2000**, *72*, 12.
(22) Kirschner, C.; Maquelin, K.; Pina, P.; Ngo-Thi, N. A.; Choo-Smith, L.-P.; Sockalingum, G. D.; Sandt, C.; Ami, D.; Orsini, F.; Doglia, S. M.; Allouch, P.; Manfait, M.; Puppels, G. J.; Naumann, D. *J. Clin. Microbiol.* **2001**, *39*, 1763.
(23) Maquelin, K.; Choo-Smith, L. P.; Endtz, H. P.; Bruining, H. A.; Puppels, G. J. *J. Clin. Microbiol.* **2002**, *40*, 594.
(24) Maquelin, K.; Kirschner, C.; Choo-Smith, L. P.; van den Braak, N.; Endtz, H. P.; Naumann, D.; Puppels, G. J. *J. Microbiol. Methods* **2002**, *51*, 255.
(25) Maquelin, K.; Kirschner, C.; Choo-Smith, L. P.; Ngo-Thi, N. A.; van Vreeswijk, T.; Stammler, M.; Endtz, H. P.; Bruining, H. A.; Naumann, D.; Puppels, G. J. *J. Clin. Microbiol.* **2003**, *41*, 324.

(26) Choo-Smith, L.-P.; Edwards, H. G. M.; Endta, H. P.; Kros, J. M.; Heule, F.; Barr, H.; Robinson, J. S.; Bruing, H. A.; Puppels, G. J. *Biopolymers* (*Biospectrosc.*) **2002**, *67*, 1.

(27) Belgrader, P.; Benett, W.; Hadley, D.; Richards, J.; Stratton, P.; Mariella, R., Jr.; Milanovich, F. *Science* **1999**, *284*, 449.

(28) Moskovits, M. *Rev. Mod. Phys.* **1985**, *57*, 783.

(29) Picorel, R.; Bakhtiari, M.; Lu, T.; Cotton, T. M.; Seibert, M. *Photochem. Photobiol.* **1992**, *56*, 263.

(30) Weitz, D. A.; Garoff, S.; Gersten, J. I.; Nitzan, A. *J. Chem. Phys.* **1983**, *78*, 5324.

(31) Kneipp, K.; Haka, A. S.; Kneipp, H.; Badizadegan, K.; Yoshizawa, N.; Boone, C.; Shafer-Peltier, K. E.; Motz, J. T.; Desari, R. R.; Feld, M. S. *Appl. Spectrosc.* **2002**, *56*, 150.

(32) Olson, L. G.; Lo, Y.-S.; Beebe, T. P., Jr.; Harris, J. M. *Anal. Chem.* **2001**, *73*, 4268.

(33) Lee, Y.-H.; Farquharson, S.; Kwon, H.; Shahriari, M.; Rainey, P. *Proc. SPIE* **1999**, *3537*, 252.

(34) Akbarian, F.; Dunn, B. S.; Zink, J. I. *J. Raman Spectrosc.* **1996**, *27*, 775.

(35) Lee, Y. H.; Dai, S.; Young, J. P. *J. Raman Spectrosc.* **1997**, *28*, 63S.

(36) Volkan, M.; Stokes, D. L.; Vo-Dinh, T. *J. Raman Spectrosc.* **1999**, *30*, 1057.

(37) Lee, Y.-H.; Farquharson, S.; Rainey, P. *Proc. SPIE* **1999**, *3857*, 76.

(38) Garcia-Rodriguez, F. J.; Gonzales-Hernandez, J.; Perez-Robles, F.; Vorobiev, Y. V., Manzano-Ramirez, A.; Jimenez-Sandoval, S.; Chao, B. S. *J. Raman Spectrosc.* **1998**, *29*, 763.

(39) Premasiri, W. R.; Clarke, R. H.; Londhe, S.; Womble, M. E. *J. Raman Spectrosc.* **2001**, *32*, 919.

(40) Farquharson, S.; Smith, W.; Lee, Y.; Elliot, S.; Sperry, J. F. *Proc. SPIE* **2002**, *4575*, 62.

(41) Nie, S.; Emory, S. R. *Science* **1997**, *275*, 1102.

(42) Kneipp, K.; Wang, Y.; Kneipp, H.; Perelman, L. T.; Itzkan, I.; Desari, R. R.; Feld, M. S. *Phys. Rev. Lett.* **1997**, *78*, 1667.

(43) Markel, V. A.; Shalev, V. M.; Zhang, P.; Huynh, W.; Tay, L.; Haslett, T. L.; Moskovits, M. *Phys. Rev. B* **1999**, *59*, 10903.

(44) Gersten, J.; Nitzan, A. *J. Chem. Phys.* **1981**, *75*, 1139.

(45) Weitz, D. A.; Garoff, S.; Gersten, J. I.; Nitzan, A. *J. Chem. Phys.* **1983**, *78*, 5324.

(46) Sokolov, K.; Chumanov, G.; Cotton, T. M. *Anal. Chem.* **1998**, *70*, 3898.

(47) Chance, R. R.; Prock, A.; Silbey, R. In *Advances in Chemical Physics, Vol. 37*; Prigogine, I., Rice, S. A., Eds.; Wiley: New York, 1978; p 1.

(48) Pineda, A. C.; Ronis, D. *J. Chem. Phys.* **1985**, *83*, 5330.

(49) Mukamel, S. *J. Chem. Phys.* **1985**, *82*, 5398.

(50) Nibbering, E. T. J.; Duppen, K.; Wiersma, D. A. *J. Chem. Phys.* **1990**, *93*, 5477.

(51) Ziegler, L. D. *Acc. Chem. Res.* **1994**, *27*, 1.

(52) Cole, J. R.; Chai, B.; Marsh, T. L.; Farris, R. J.; Wang, Q.; Kulam, S. A.; Chandra, S.; McGarrell, D. M.; Schmidt, T. M.; Garrity, G. M.; Tiedje, J. M. *Nucleic Acids Res.* **2003**, *31*, 442.

(53) Helgason, E.; Okstad, O. A.; Caugant, D. A.; Johansen, H. A.; Fouet, A.; Mock, M.; Hegna, I.; Kolsto, *Appl. Environ. Microbiol.* **2000**, *66*, 2627.

(54) Rothschild, K. J.; Andrew, J. R.; DeGrip, W. J.; Stanely, H. E. *Science* **1976**, *191*, 1176.

(55) Susi, H.; Sampugna, J.; Hampson, J. W.; Ard, J. S. *Biochem.* **1979**, *18*, 297.

(56) Kearns, D. B.: Losick, R. *Mol. Microbiol.* **2003**, *49*, 581.

(57) In this *cotE::cat B. anthracis* mutant, the chloramphenicol-resistance gene chloramphenicol transacetylase replaces most of the *cotE* gene rendering it nonfunctional.

(58) Sockalingum, G. D.; Beljebbar, A.; Morjani, H.; Angiboust J. F.; Manfait, M. *Biospectroscopy* **1998**, *4* (5 Suppl.), S71.